Fountain fringe field switching (FFFS) for wide viewing angle LCDs

Journal of Physics D: Applied Physics

PAPER • **OPEN ACCESS**

Fountain fringe field switching (FFFS) for wide viewing angle LCDs

To cite this article: Lachezar Komitov *et al* 2022 *J. Phys. D: Appl. Phys.* **55** 185102

OPEN ACCESS
IOP Publishing
Journal of Physics D: Applied Physics
J. Phys. D: Appl. Phys. **55** (2022) 185102 (13pp)
https://doi.org/10.1088/1361-6463/ac4dc9

Fountain fringe field switching (FFFS) for wide viewing angle LCDs

Lachezar Komitov[1,2,3], Giovanni Barbero[4,5], Mohammed Ibn Elhaj[3], Przemysław Morawiak[6] and Wiktor Piecek[6,*]

[1] University of Gothenburg, SE-41296 Gothenburg, Sweden
[2] Innovidis AB, PO 3029, 40010 Gothenburg, Sweden
[3] HighVisTec GmbH, Benkenstrasse 254C, CH 4108 Witterswill, Switzerland
[4] DISAT Politecnico di Torino, Corso Duca degli Abruzzi 24, 10129 Torino, Italy
[5] National Research Nuclear University MEPHI (Moscow Engineering Physics Institute), Kashirskoye shosse 31, 115409 Moscow, Russia
[6] Military University of Technology, Kaliskiego St 2, 00-908 Warszawa, Poland

E-mail: wiktor.piecek@wat.edu.pl

Received 4 October 2021, revised 15 December 2021
Accepted for publication 21 January 2022
Published 4 February 2022

Abstract

To reduce or completely remove the viewing angle dependence of liquid crystal (LC) displays and devices, we have recently introduced a new electrode structure for LC displays. This electrode structure has openings (holes) in the pixel electrode (PixE) for generating fringe electric field with azimuthal degenerated distribution of the field lines around each hole, resembling a fountain. Such a field is promoting azimuthally degenerated switching of the LC molecules and thus generation of images with 360° viewing angle constant contrast when a pair of crossed circular polarisers are used. A theoretical model of the fountain fringe field, generated around a single circular hole and plurality of such holes in the PixE, is presented.

Keywords: perforated electrode, fountain fringe field, wide azimuthal viewing angle

(Some figures may appear in color only in the online journal)

1. Introduction

Liquid crystal (LC) materials consist of molecules with anisotropic shape. Due to their long-range molecular order LCs exhibit anisotropic physical properties, such as dielectric, magnetic, optical, etc. LC materials are ubiquitous used today in variety of displays and photonic devices. In the majority of the conventional liquid crystal displays (LCDs), the generated optical images are due to the LC optical anisotropy, i.e. their optical birefringence. These images, however, exhibit usually a limited viewing angle as well as they may exhibit inversion of the contrast and color shift, which is well described in the literature [1].

For many display applications of the LCs, wide viewing angle with high constant contrast, is required. For obtaining of a desirable device performance, however, a variety of combinations of different optical films are used in LCD architecture for compensating a poor viewing angle characteristics [2, 3]. As a result, the complexity and the cost of the LCDs becomes high.

Another successful approach to reduce efficiently the viewing angle dependence of LCDs, is to create a multidomain structure of the LC alignment in the single LCD pixel area and/or patterning the electrodes so that they generated over the pixel a degenerated LC alignment, which is reducing the viewing angle dependence [4, 5]. Both these approaches have their advantages and disadvantages. In the case of patterned electrodes, since the applied electric field orients the LC molecules accordingly, a patterned alignment of the LC

* Author to whom any correspondence should be addressed.

molecules corresponding to the field pattern, will be obtained. Hence, by choosing appropriate electrode pattern, a proper LC field-induced alignment configuration could be generated, which is providing enlarging the viewing angle dependence of the images generated by the LCD.

In this work, we present a new layered electrode structure for generating a fringe field (FF), which is consisting of a common electrode (CE) and second pixel electrode (PixE) with holes. Both electrodes are deposited on one of the cell's substrates and are separated from each other by an insulation layer (figure 1(a)). The layered electrode with such a structure we call a perforated electrode (PE). This PE structure, as we shall see, generates a FF around each hole in the PixE, which configuration resembles a fountain (fountain fringe field or FFF). The performance of a LCD, containing a similar electrode structure, was computer simulated in [6, 7]. The idea of PE electrode structure in LC devices was first introduced by us in 2007 [8]. The principle and performance of LC devices with PE electrode, for generating FFF, were also partially presented at IDW'20 [9]. Further development of the PE electrode concept was recently described in [10].

In this work, we studied experimentally the reorientation of the LC in a cell, with initially field-off vertical alignment (VA) (figure 1(b)) by the FFF, generated by PE (figure 1(b)). Such reorientation of the molecules of LC with $\varepsilon_a > 0$ from field-off VA state to fountain resembling configuration (field-on state) (figure 1(c)), which we call FFF switching (FFFS). FFFS enables to generate images with near 360° azimuthal viewing angle at constant contrast. For accelerating the relaxation process of the LC to the initial field-off VA state, we employed a second ITO counter electrode (top electrode—TE) in the cell, which is deposited on the cell substrate facing the substrate with PE. Applying voltage to the PE and TE, an electric field is generated electric field across the LC layer, which is improving the turn-off time τ_{fall} of the cell [11, 12].

We present also a theoretical model of the FFF considering the case of PE with circular micron-sized holes in the PixE. We describe the configuration of FFF generated around a single hole in the PixE as well as the one generated by a square lattice of holes. Such FFF orients the molecules of the LC with positive dielectric anisotropy $\varepsilon_a > 0$ along the field lines, resulting in 360° azimuthally degenerated alignment of the LC molecules around the holes in the PE, resulting to a hemispherical-like viewing angle.

2. Experiment and results

The experimental cell is of conventional sandwich type, consisting of two parallel glass plates separated at predefined distance, usually several microns (3 and 4 μm). One of the cell substrates is covered with continuous ITO (indium tin oxide) electrode, TE, playing the role of counter electrode, whereas on the other substrate is deposited PE, for generating FFFs. Such three-electrode structure is described in [8, 9] and in our case is consisting of CE and PixE with holes, forming PE, deposited on one of the cell substrates and continuous ITO electrode (TE) on the other substrates, respectively. Three electrode structure was aimed to reduce the fall time τ_{fall} of the LC cell. The PE for generating FFF consisted of common ITO electrode (CE), covered by thin insulation layer SiO_2 (200 nm), on top of which is deposited second ITO electrode, representing the PixE (figures 1 and 2). The PixE contains circular micron size holes, which are separated from each other and are uniformly distributed over the whole pixel area (cf figure 2). The diameter of the holes in the PE in our cell was 5 μm and the distance between the holes is also 5 μm. The inner surface of the cell substrates is covered with alignment layer SE1211 (kindly supplied by Nissan Chemical Industries, Ltd), which promotes high quality homeotropic alignment (VA) of the LC molecules in the field-off state (see figure 1(a)). The experimental cell was filled under vacuum with the nematic LC mixture MDA-09-2329 (kindly supplied by Merck) with $\Delta\varepsilon = 21.2$ at room temperature. After filling, the cells were heated up to isotropic phase and slowly cooled down to room temperature. The quality of the vertical alignment of the LC in the cells was inspected in polarizing microscope between crossed polarisers. All cells were found to exhibit high quality dark state between the crossed polarisers, thus proving the uniform field-off vertical alignment of the LC in the cells.

The electro-optic response of these cells was investigated in a conventional set-up for studying the electro-optic response of LC devices, consisting of polarizing microscope with a camera, photodetector unit with amplifier, power supply and oscilloscope. All devices are connected to a computer with appropriate software for collecting and analyzing data.

The FFFS was studied in one pixel cell with size 5 × 5mm PE (see figure 3). The field-off state of the LC was vertical, i.e. the LC molecules were aligned along the substrate normal (figures 1(b) and 15(a)). Therefore, the cell inserted between the crossed linear polarisers of the polarizing microscope appeared completely dark in this state. When applying an electric field between the CE and the PixE, FFF is generated around the holes, which in turn resulted in FFFS of the LC transforming the initial vertical alignment of the LC to azimuthally degenerated around each pixel hole (see figure 15(b)). As we shall see, this makes possible the generation of images with possible 360° azimuthally independent viewing angle and constant contrast when the cell is inserted between crossed circular polarisers.

The FFFS of the nematic LC in the experimental cell is presented in figure 3, where the photographs of the cell were taken at four different positions of the cell between two crossed linear polarisers are shown. The dark area of the photographs corresponds to the cell area outside of the pixel, in which the LC molecules have vertical alignment, whereas the bright area corresponds to the pixel area where the FFFS of the LC took place.

The measured contrast ratio of the cell was 1:1500. As seen, from figure 3 the contrast between the field-off area outside of the pixel (dark part) and field-on area of the pixel (bright part), remains constant during the rotation of the cell between the crossed linear polarisers. Hence, the dark and bright state, respectively, appears to be with isotropic in-plane optical properties, which is exactly the prerequisite for generating

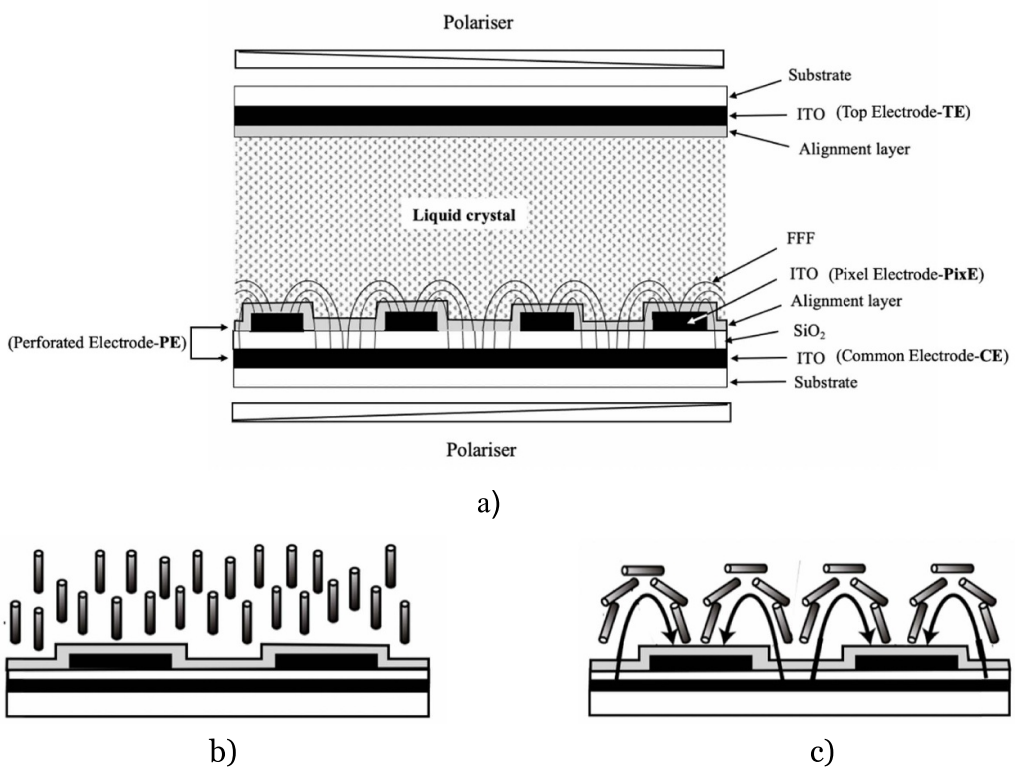

Figure 1. Schematic presentation of the experimental cell cross section. Alignment of the LC molecules (at the substrate surface bearing the FFF electrode only) in (a) field-off state and (b) field-on alignment configuration of the LC molecules due to FFFS (cf figures 12(b) and (c)).

images by FFFS with wide azimuthal viewing angle, and, as we shall see, it will become 360° with constant contrast when the cell is inserted between crossed circular polarisers instead of linear.

The rise time τ_{rise} of the cell was measured when applying electric field between the PixE and the CE. It was measured $\tau_{\text{rise}} = 2.0$ ms at applied voltage 13.0 V_{pp}. The fall time τ_{fall}, of the cell, due to elastic relaxation of the LC taking place after the electric field between the pixel and CE was turned off, was measured to be 5.8 ms. However, if, after switching off the electric field applied between the pixel and CE, an electric field is applied between the electrodes deposited onto inner substrates surfaces of both substrates, i.e. between the counter ITO electrode and the PE (containing the PixE and CE), then τ_{fall} was reduced to 2.5 ms.

3. Theory

3.1. FF generated by preforated PixE

3.1.1. Electric field generated by a single hole in the PE. The goal of the calculation presented below is the determination of the electric field E created by a system formed by two overlapping parallel electrodes, separated by a distance d, connected to a power supply fixing a difference of potential between them of ΔV. One of the electrodes is a standard electrode, represented by a plan, which we call CE.

The other electrode, so called PixE, is presented by a perforated plane consisting in a periodic distribution of identical circular holes, of radius R. We call this electrod PixE. As reported herein, an electrode configuration of this type was used to control the optical transmission of a sandwich cell, filled with nematic liquid crysatl with $\varepsilon_a > 0$, where the LC molecules, by approprate surface treatment, were oriented along the substrate normal (VA), In the absence of electric field applied between the two electrodes, common CE and PixE, the VA in the cell is stable and between crossed polarizer the cell is not transmitting the incident light (black state). When a difference of potential between the these two electrodes is applied, a fringe electric field (FF) is generated outside the electrodes, due to the presence of the holes in the PixE. The FF induces elastic deformation of the nematic LC, which pattern corresponds to the one of the FF generated around the holes and the incoming light is passing through the cell, bright state.

To determine the electric field E we take advantage of the superposition principle. We begin the calculation considering a flat parallel condenser, of infinite surface area, of gap d between the electrodes (figure 4). The cartesian reference frame used for the description has the (x,y)-plane parallel to the electrodes, situated at $z = 0$, and $z = -d$. We assume that the the positive electrode is at $z = -d$. When the difference of potential between the electrodes is ΔV, the electric field is:

$$E_0 = \frac{\Delta V}{d} u_z, \quad \text{for} \quad -d \leq z \leq 0, \tag{1}$$

$$E_0 = 0, \quad \text{for } z \langle -d, \quad \text{and } z \rangle 0 \tag{2}$$

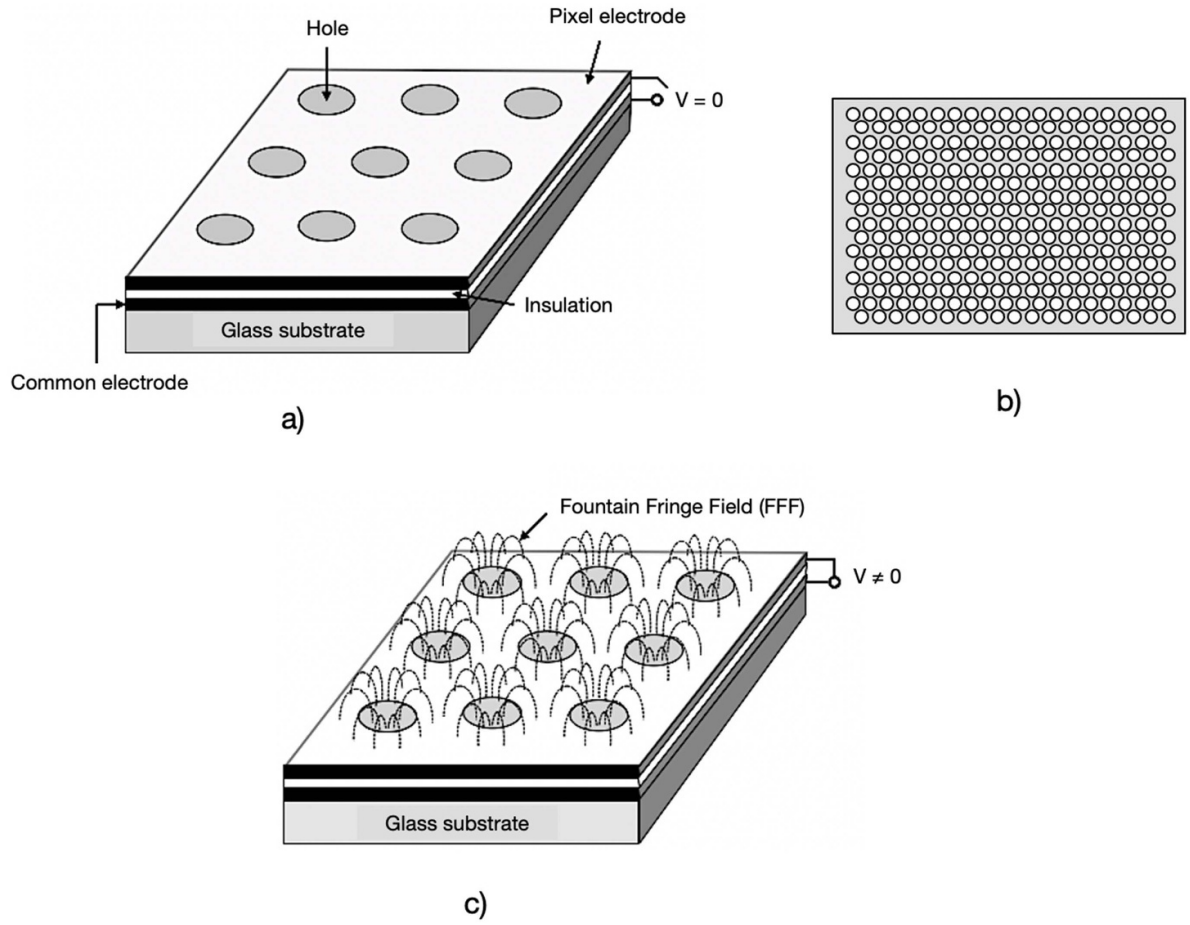

Figure 2. Schematic presentation of the layered electrode structure for generating FFs over the PixE. (a) Overlook of the layered electrode (PE) in field-off state ($V = 0$), (b) the PixE of the layered electrode structure, containing micron size circular holes evenly distributed over the PixE and separated from each other at distance approximately equal to the hole diameter. (c) Overlook of the PE in the field-on state ($V \neq 0$), showing the electric field lines distribution. Around each hole in the PixE is generated FF, resembling a fountain. Therefore, the generated FF around the holes we call FFF. Reproduced from [9]. [Virtual conference IDW'20, 9–11 December 2020, Proceedings of the International Display Workshops, vol 27, pp 26–27 (2020)].

as well known from elementary electrostatics. The unit vector u_z is the along the z-axis. The surface density of electric charge σ responsible for the electric field is $\sigma = \varepsilon_0 E_0 = \varepsilon_0 (\Delta V/d)$.

Let us consider now the situation in which the upper electrodes, carrying the charge density $-\sigma$, presents a hole centered on the z-axis at $z = 0$. The resultant electric field, E, for the superposition principle is the sum of the field due to the condenser where the hole is absent, E_0, plus the electric field of a disc carrying the charge density σ, located in the position of the hole, E_D. In fomula:

$$E = E_0 + E_D. \tag{3}$$

Since we are interested in the electric field in the region occupied by the nematic LC, where $E_0 = 0$, it follows from (3) that the electric field we are looking for is simply the electric field due to the disc.

On the axis of the disc, for symmetry reasons, the electric field has only a component along the z-axis given by:

$$E(z) = \kappa z \left(\frac{1}{|z|} - \frac{1}{\sqrt{z^2 + R^2}} \right) u_z, \tag{4}$$

where $\kappa = \sigma/(2\varepsilon_0) = \Delta V/(2d)$.

As it is well known, on the z-axis, the electric field E presents a discontinuity at $z = 0$ of the normal component. In a point lying not on the axis of the disc, the electric field has also, a component, parallel to the plane of the disc. This component is continuous across the plane $z = 0$. To evaluate the electric field in the region occupied by the LC, we operate in the following manner.

The electric field created by the disc E_D in a point P of coordinates (x, y, z) has the cartesian components [13].

$$E_x(x,y,z) = k \int_{-R}^{R} \mathrm{d}x' \int_{-\sqrt{R^2 - x'^2}}^{\sqrt{R^2 - x'^2}} \times \frac{x - x'}{\left[(x - x')^2 + (y - y')^2 + z^2\right]^{3/2}} \mathrm{d}y', \tag{5}$$

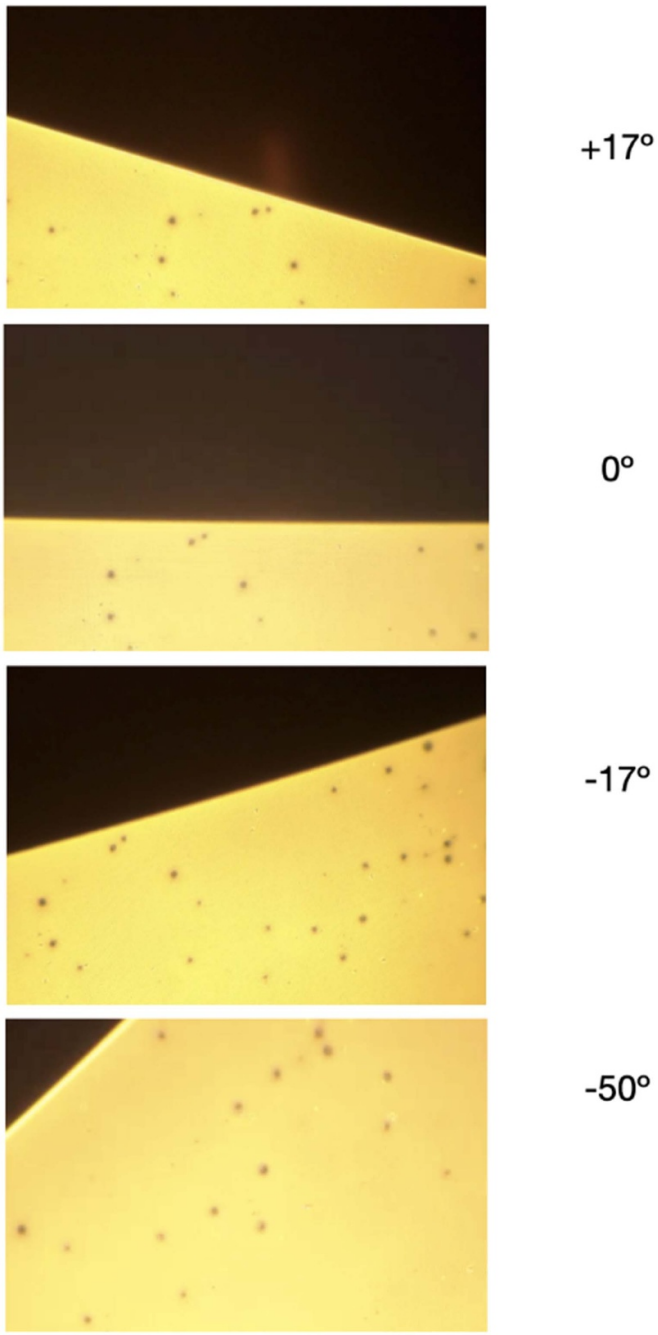

Figure 3. Photographs of one-pixel LC cell, shown in figure 1, inserted in the polarizing microscope between two crossed linear polarisers. The cell is in field-on state, demonstrating FFFS of the LC. The black area is the one out of the layered FFF electrode (field-free state). The images are taken at different angles of rotation of the cell between the crossed polarisers. Reproduced from [9]. [Virtual conference IDW'20, 9–11 December 2020, Proceedings of the International Display Workshops, vol 27, pp 26–27 (2020)].

$$E_y(x,y,zz) = k\int_{-R}^{R} \mathrm{d}x' \int_{-\sqrt{R^2-x'^2}}^{\sqrt{R^2-x'^2}} \times \frac{y-y'}{\left[(x-x')^2+(y-y')^2+z^2\right]^{3/2}}\,\mathrm{d}y', \quad (6)$$

$$E_z(x,y,z) = k\int_{-R}^{R} \mathrm{d}x' \int_{-\sqrt{R^2-x'^2}}^{\sqrt{R^2-x'^2}} \times \frac{z}{\left[(x-x')^2+(y-y')^2+z^2\right]^{3/2}}\,\mathrm{d}y', \quad (7)$$

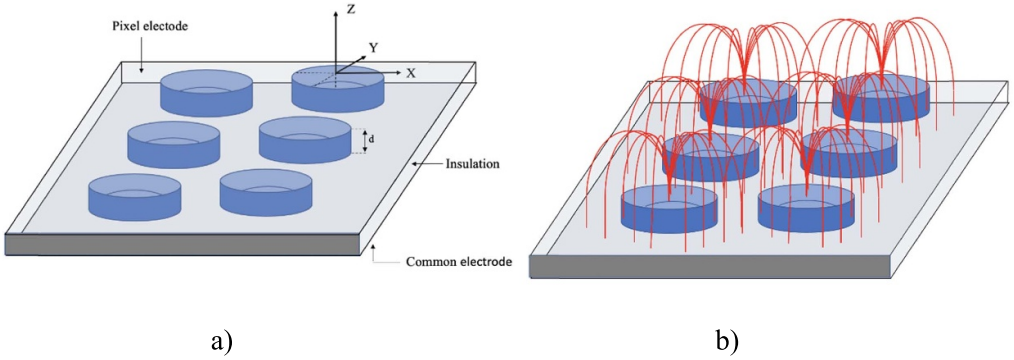

Figure 4. Schematic presentation of the PE with the related coordinate system. The generated FF around each hole in the PixE.

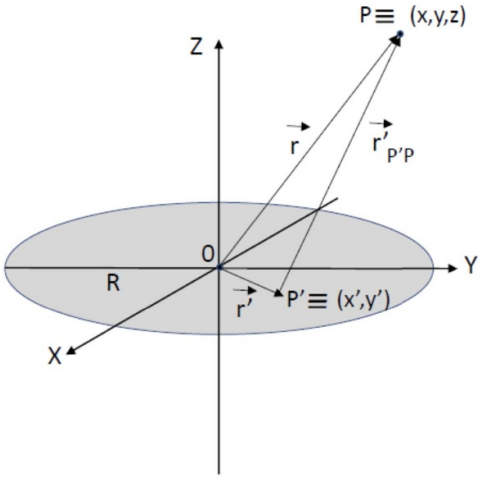

Figure 5. Cartesian reference system and symbols used for the description of the electric field E created by a circular hole.

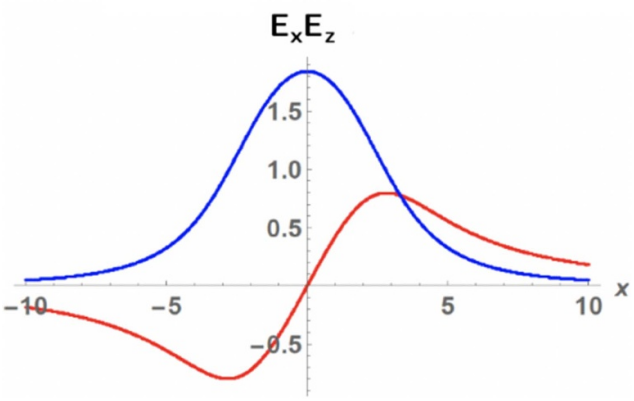

Figure 6. Cartesian components E_x (in red) and E_z (in blue) of the electric field $E(r)$ created by a disc (lying in the (x,y)-plane), uniformly charged with the density σ, versus the distance x from center of the hole (z-axis), in the range $a \leq x \leq a$, where $a = 10\,\mu$m at $z = R$.

where (x',y'), indicate a generic point of the disc contributing to the electric field E_D in arbitrary chosen point $P(r)$, see figure 5, and $k = \sigma/(4\pi\varepsilon_0) = \kappa/(2\pi)$. In the simple case in which $P(r)$ is on z-axis, a simple calculation gives:

$$E_x(0,0,z) = 0,\ \ E_y(0,0,z) = 0, \text{ and } E_z(0,0,z) = \kappa z\left(\frac{1}{|z|} - \frac{1}{\sqrt{z^2+R^2}}\right), \tag{8}$$

as reported above.

For points $P(r)$ out of the z-axis the generated fringe electric field E_D has E_x and E_y components and cylindrical symmetry around the z-axis, as it will be discussed later. In the following we present a few simulations of the E_x and E_z component of the electric field $E(r)$, on the (x,z)-plane. For the calculation we assume the radius of the single hole as $R = 2.5\,\mu$m.

In figure 6 we show the components parallel to the disk plane, E_x, and perpendicular to it, E_z, versus x-coordinate in the range $-a \leq x \leq a$, where $a = 10\,\mu$m, at $z = R$. The componets of electric field are in $\Delta V/4\pi d$ units, As expected, E_x is continuous at $x = 0$. The amplitude $|E_x|$ presents a maximum out of the hole. On the contrary, E_z presents a maximum at $x = 0$, and decreases monotonically as $|x|$ increases.

In figure 7, the components of the electric field E_x and E_z are presnted versus z, at (a) $x = 0.5 \times R$, and (b) $x = 1.5 \times R$.

Note that, the component E_z presents a discontinuity at $z = 0$ if $x < R$, whereas it is continuous at $x > R$. On the contrary, E_x is always continuous at the disc surface (at $z = 0$).

3.1.2. Electric field generated E(r) *by plurality of holes in the PE.* The calculation reported above was relevant to a single hole, centered in the origin of the cartesian reference frame, on the (x,y)-plane. The FF generated by a single hole, as presented above, has cylindrical symmetry around the z-axis with field lines forming a fountain centered on the hole. To extend the calculation to our case, we consider a surface distribution of holes, forming a square lattice of spatial period a. The generic hole has the center in the point C_{ij} of cartesian coordinates $C_{ij} = (ia, ja, 0)$, where i and j are two integer numbers.

The vector $r = (x,y,z)$ indicates the position of the point P, in which we evaluate the electric field $E(r)$. A generic point inside the hole (i,j) has relative coordinates with respect to C_{ij}, (x',y'), and its vector position is ${r_{ij}}' = (x',y')$, where, as before, $|x'| \leq R$ and $|y'| \leq R$ (see figure 8).

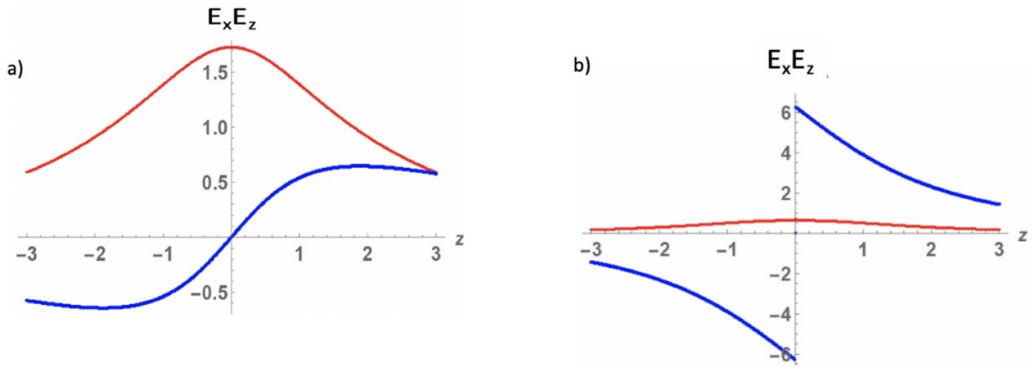

Figure 7. Cartesian components E_x (in red) and E_z (in blue) of the electric field $E(r)$ created by a disc (lying in the (x,y)-plane), uniformly charged with the density σ, versus the distance x from center of the hole (z-axis) at (a) $x = 0.5 \times R$, and (b) $x = 1.5 \times R$. Note that E_x is continuous for $z = 0$, whereas E_z presents a discontinuity if $x < R$, whereas it is continuous if $x > R$.

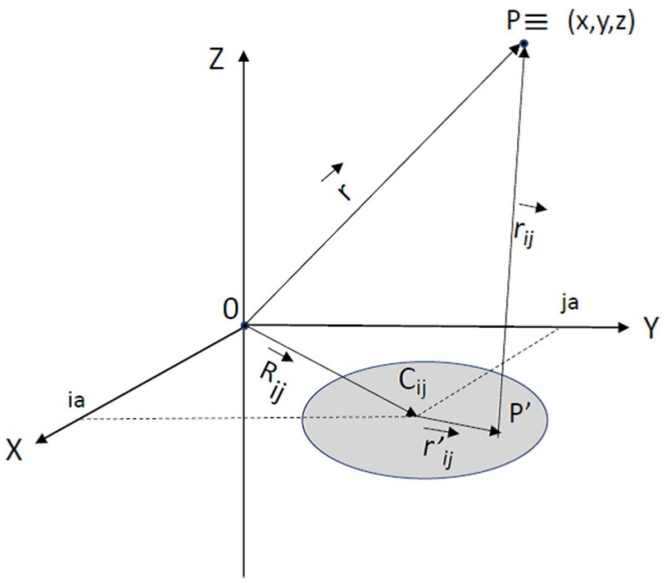

Figure 8. Cartesian reference system and symbols used for the description of the electric field $E(r)$ created by a square lattice of holes in PixE.

The vector position of C_{ij} with respect to the origin of the cartesian reference frame is given by $R_{ij} = (ia, ja)$. It follows that r, in terms of R_{ij}, r_{ij} and $r_{ij}{}'$ can be written as:

$$r = R_{ij} + r_{ij}{}' + r_{ij}$$

from which we get:

$$r_{ij} = r - r_{ij}{}' - R_{ij}$$

where

$$r_{ij} = (x - x' - ia, y - y' - ja, z)$$

and

$$r_{ij} = \sqrt{(x - x' - ia)^2 + (y - y' - ja)^2 + z^2}.$$

The electric field $E_{ij}(r)$ due to the hole of center C_{ij} in r is:

$$E_{ij}(x,y,z) = k \int_{-R}^{R} \mathrm{d}x \int_{-\sqrt{R^2-x'^2}}^{\sqrt{R^2-x'^2}} \frac{r_{ij}}{r_{ij}^3}\,\mathrm{d}y'.$$

The total electric field due to the distribution of the holes is then:

$$E(x,y,z) = \sum_{i,j} E_{ij}(x,y,z),$$

whose cartesian components are:

$$E_x(x,y,z) = k \int_{-R}^{R} \mathrm{d}x' \int_{-\sqrt{R^2-x'^2}}^{\sqrt{R^2-x'^2}} \mathrm{d}y' \times \sum_{i,j} \frac{x - x' - ia}{\left(\sqrt{(x - x' - ia)^2 + (y - y' - ja)^2 + z^2}\right)^3}, \tag{9}$$

$$E_y(x,y,z) = k \int_{-R}^{R} \mathrm{d}x' \int_{-\sqrt{R^2-x'^2}}^{\sqrt{R^2-x'^2}} \mathrm{d}y' \times \sum_{i,j} \frac{y - y' - ja}{\left(\sqrt{(x - x' - ia)^2 + (y - y' - ja)^2 + z^2}\right)^3}, \tag{10}$$

$$E_z(x,y,z) = k \int_{-R}^{R} \mathrm{d}x' \int_{-\sqrt{R^2-x'^2}}^{\sqrt{R^2-x'^2}} \mathrm{d}y' \times \sum_{i,j} \frac{z}{\left(\sqrt{(x - x' - ia)^2 + (y - y' - ja)^2 + z^2}\right)^3}. \tag{11}$$

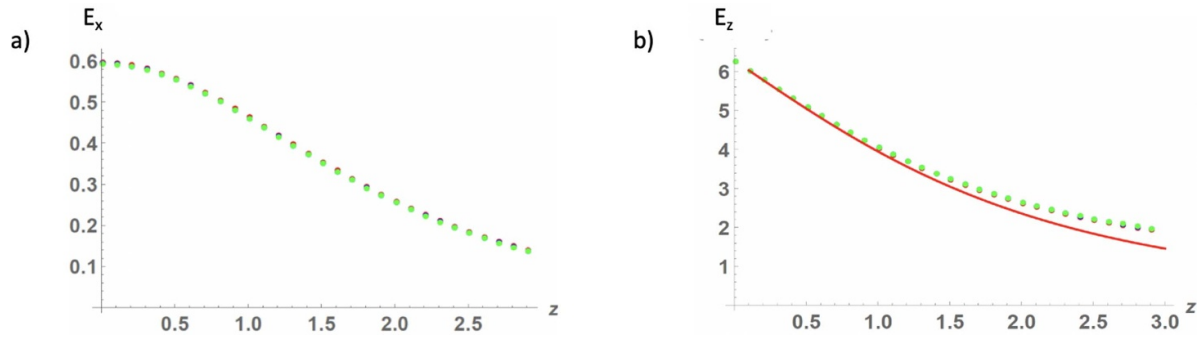

Figure 9. Cartesian components E_x and E_z of the electric field $E(r)$ created by a uniformly charged disc versus the distance z from the the (x,y)-plane containing the hole, at a distance from the axis of the hole $x = 0.5 \times R$. (a) E_x and (b) E_z. Red points, $-5 \leq (i,j) \leq 5$, blue points, $-10 \leq (i,j) \leq 10$, green points $-15 \leq (i,j) \leq 15$, black points $-100 \leq (i,j) \leq 100$. As seen, all points collapsed in one within $-5 \leq (i,j) \leq 5$. On the figure (b) is shown also $E_z(z)$ evaluated on the axis by a single hole (red curve).

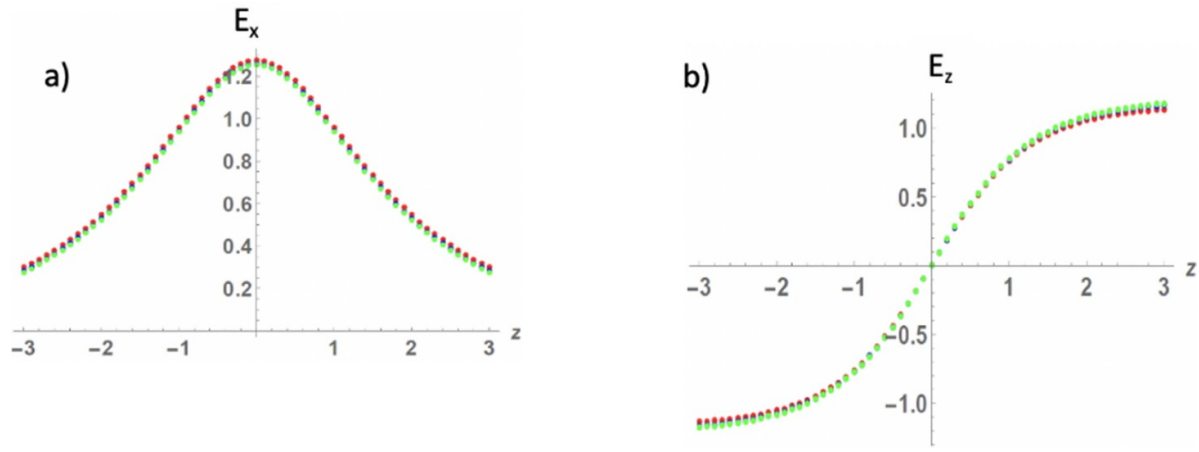

Figure 10. Cartesian components E_x and E_z of the electric field $E(r)$ created by a distribution of discs uniformly charged versus the distance from the the (x,y)-plane containing the hole, at a distance from the axis of the hole $x = 1.5 \times R$. (a) $E_x(z)$ and (b) $E_z(z)$. Red points, $-5 \leq (i,j) \leq 5$, blue points, $-10 \leq (i,j) \leq 10$, green points $-15 \leq (i,j) \leq 15$, black points $-100 \leq (i,j) \leq 100$. Likewise in figure 5, all points collapsed in one within $-5 \leq (i,j) \leq 5$.

In figure 9 the components of the electric field evaluated summing the contributions from the holes, with different approximations are shown versus the distance from the (x,y)-plane, for $y = 0$ and $x = 0.5 \times R$.

In figure 10 the components of the electric field E_x and E_z evaluated summing the contributions of the holes, with different approximations are shown versus the distance from the (x,y)-plane, at $y = 0$ and $x = 1.5 \times R$. As it is evident from figures 5 and 6 already with $-5 \leq (i,j) \leq 5$ the approximation is sufficiently good.

In figure 11 we show the x-dependence, in the range $-a \leq x \leq a$, of the cartesian components of the electric field, E_x (a) and E_z (b) due to the distribution of holes with the the analogous components due to a single hole, centered in the origin of the reference frame (center of the hole).

As it is evident from figure 11, inside the hole the field is only slighted perturbed by the distribution. However, outside the effect of the distribution, imposing the periodicity of the effective electric field, is important. As it will be shown in the appendix, the cylindrical symmetry around the z-axis passing from the center of the electrode is conserved also in the case of a distribution of holes on a square lattice. This result is of some importance for what concerns the interaction between the electric field and the LC anisotropy.

In fact, the interaction energy density related to the presence of the external field with the nematic LC described by the average molecular orientation n is given by:

$$f_E = -\frac{1}{2}\varepsilon_a (n \cdot E)^2, \tag{12}$$

where $\varepsilon_a = \varepsilon_{\parallel} - \varepsilon_{\perp}$, in which $\parallel$ and $\perp$ refer to the director n. It follows that, in the case $\varepsilon_a > 0$, the nematic director n tends to be oriented along the local electric field, giving rise to the fountain pattern of the LC alignment. Computer simulation of FFFS a cell with PE and initial vertical alignment is presented in figure 15. Hence, the LC molecules adopt azimuthally degenerated alignment around the holes in the PixE, thus provided in-plane optically isotropic properties of the LC device with perforated PixE.

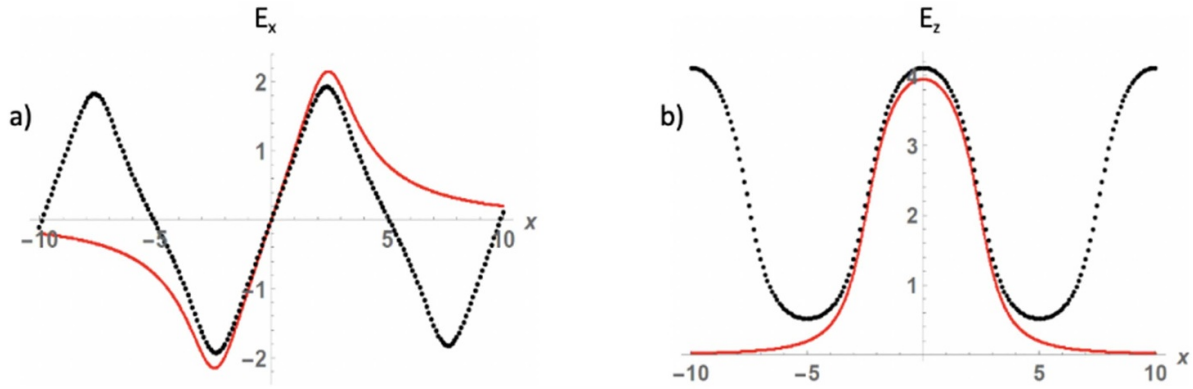

Figure 11. Cartesian components E_x and E_z of the electric field $E(r)$ created by a disc uniformly charged in red, versus x, in the range $(-a \leq x \leq a)$ at a distance $z = R$ from the (x,y)-plane containing the hole, compared with the cartesian components due to a distribution of holes, in black, (a) $E_x(x)$ and (b) $E_z(x)$, contained in $-100 \leq (i,j) \leq 100$.

4. Discussion and conclusion

To omit the azimuthal angular dependence of the viewing angle of the images generated by LC displays and devices, is not a trivial task. There are several known methods, which are partially but not completely able to suppress this dependence. Usually, a proper combination of optically compensating plates and/or technology, providing patterning of the alignment layer in the LCDs or the one of the applied electric field is required. In this work, we reported on a new approach, according to which the LC in the cell is switched by an electrode, constituting of CE, insulation layer and PixE, containing a plurality of holes with micron size. This electrode, which we call PE, is generating FF around each hole, which lines distribution resembles a fountain (cf figure 12). The LC studied in this work has $\varepsilon_a > 0$ and vertical field-off alignment. In the cell. Therefore, when applying voltage to the PE, the VA of the LC is switched by the FF to an alignment having the same configuration as the field lines of the FF, i.e. the LC is switched from vertical to a fountain-like configuration. We, therefore, call this kind of switching FFFS. The holes in the PixE in our experimental cells have a circular form and are evenly distributed over the pixel area as it is demonstrated in the computer simulations of the FFFS depicted in figure 12. Therefore, the FFFS enables generation of images with 360° viewing angle with constant contrast when the cell is inserted in between two crossed circular polarisers, as demonstrated below.

To study the FFFS, the experimental cell, depicted in figure 1, is inserted in the polarizing microscope between linear or crossed polarisers. In field-off state the cell is not transmitting the incident light and therefore it is in black state. However, applying a voltage to the cell, a FFFS of the LC take place and the light is transmitted through the cell and the crossed polarisers and the cell switches to bright state. In figure 13(a) is shown photograph of a magnified area of the experimental cell taken in polarizing microscope with crossed linear polarisers. As seen from the figure, circular domains are formed around each circular hole (red circle), due to the FFFS. These domains are centered with the holes in the PixE. In the figures 13(b) and (c) are shown computer simulated images

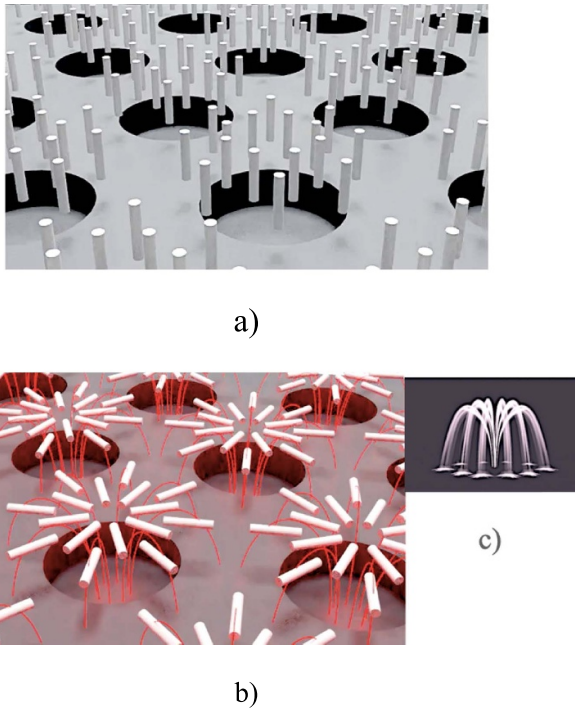

Figure 12. Computer simulation of the FFFS in a cell containing nematic LC with $\varepsilon_a > 0$. (a) In the field-off state, LC molecules are oriented along the substrate normal (vertical alignment). (b) In the field-on state, the generated FF around each hole in the PixE orients the LC molecules along the field lines, which 3D distribution, resembles a fountain (i.e. FFF). (c) Therefore, the LC switching by the FFFs we call FFFS. Reproduced from [9]. [Virtual conference IDW'20, 9–11 December 2020, Proceedings of the International Display Workshops, vol 27, pp 26–27 (2020)].

of such a cell between crossed linear and circular polarisers, respectively.

These simulations showed that the intensity of the transmitted light through the cell and the crossed circular polarizer is twice higher than when linear crossed polarisers are used instead. Moreover, the generated images by the FFFS in the cell inserted in between circular polarisers exhibit 360°

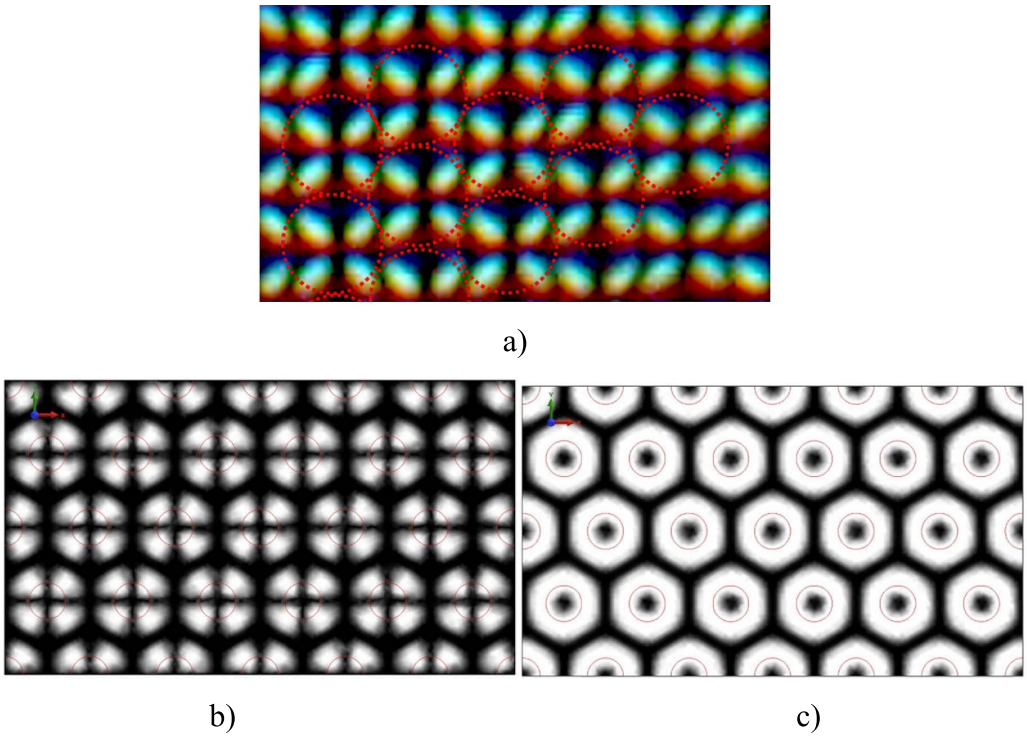

Figure 13. (a) Photograph of the experimental cell under polarising microscope with crossed linear polarisers. The red circles in the photo are for guiding the eyes and correspond to the circular holes in the PixE. Computer simulations of the field-on state of the cell viewed between crossed (b) linear and (c) circular polarisers, respectively [10].

azimuthal viewing angle with constant contrast, whereas the images generated, when linear polarisers are used, without any optical compensation, the contrast is reduced significantly when the azimuthal viewing angle is along the transmission directions of the polarisers.

Moreover, the generated images by the FFFS in the cell inserted in between circular polarisers exhibit 360° azimuthal viewing angle with constant contrast, whereas the images generated, when linear polarisers are used, without any optical compensation, the contrast is reduced significantly when the azimuthal viewing angle is along the transmission directions of the polarisers. The counter ITO (3rd) electrode TE may significantly reduce the τ_{fall} and thus will further advance the performance of the device having such a three-electrode structure consisting of CE, PixE with holes for generating FFF, and counter ITO electrode.

In conclusion, the studied in this work FFFS, which was generated in the LC cells containing PE, shows a great potential for applications in LC displays and devices. It enables the switching of the LC to a state having 360° azimuthal degeneration of the LC molecules' alignment around the holes in the PixE and thus enabling generation of images with 360° azimuthal viewing angle and constant contrast. The FFFS appears also appropriate for applications in other LCDs modes than those based on ECB mode, for instance those which do not require any polarisers, such as guest-host effect, cholesteric bistable LCDs, light scattering LCDs, etc. The employment of PEs generating FFFS in these LCDs would be highly advantageous for the quality of their performance.

Data availability statement

The data that support the findings of this study are available upon reasonable request from the authors.

Acknowledgments

We are grateful to Dr Melanie Klasen-Memmer, Merck, for the kind support of our research with LC materials. Professor Giovanni Barbero was partially supported by National Research Nuclear University MEPHI (Moscow Engineering Physics Institute).

The project was supported with funds of MUT Grant UGB 22-843.

Appendix. Symmetry of the electric field

In the case of a single hole, the cartesian components of the electric field $E(r)$ are given by equations (5)–(7). As discussed above, the electric field $E(r)$ has cylindrical symmetry around the z-axis, coinciding with the axis of the hole. In order to show the cylindrical symmetry of the electric field created by a single hole with respect to the z-axis passing for the centre of the electrode, we have to take into account that the cartesian components of the electric field are given by equations (5)–(7). From these expreesions it follows that:

$$E_x(x,y,z)+E_x(-x,-y,z)=k\int_{-R}^{R}\mathrm{d}x'\int_{-\sqrt{R^2-x'^2}}^{\sqrt{R^2-x'^2}}\times\Phi_x(x,y,z;x',y')\,\mathrm{d}y', \quad (13)$$

$$E_y(x,y,z)+E_y(-x,-y,z)=k\int_{-R}^{R}\mathrm{d}x'\int_{-\sqrt{R^2-x'^2}}^{\sqrt{R^2-x'^2}}\times\Phi_y(x,y,z;x',y')\,\mathrm{d}y', \quad (14)$$

$$E_z(x,y,z)-E_z(-x,-y,z)=k\int_{-R}^{R}\mathrm{d}x'\int_{-\sqrt{R^2-x'^2}}^{\sqrt{R^2-x'^2}}\times\Phi_z(x,y,z;x',y')\,\mathrm{d}y', \quad (15)$$

where, as it follows from equations (5)–(7),

$$\Phi_x(x,y,z;x',y')=\frac{x-x'}{\left[(x-x')^2+(y-y')^2+z^2\right]^{3/2}}-\frac{x+x'}{\left[(x+x')^2+(y+y')^2+z^2\right]^{3/2}}, \quad (16)$$

$$\Phi_y(x,y,z;x',y')=\frac{y-y'}{\left[(x-x')^2+(y-y')^2+z^2\right]^{3/2}}-\frac{y+y'}{\left[(x+x')^2+(y+y')^2+z^2\right]^{3/2}}, \quad (17)$$

$$\Phi_z(x,y,z;x',y')=\frac{z}{\left[(x-x')^2+(y-y')^2+z^2\right]^{3/2}}-\frac{z}{\left[(x+x')^2+(y+y')^2+z^2\right]^{3/2}}. \quad (18)$$

A simple inspection of (5)–(7) reveals that:

$$\Phi_x(x,y,z;x',y')=-\Phi_x(x,y,z;-x',-y'), \quad (19)$$

$$\Phi_y(x,y,z;x',y')=-\Phi_y(x,y,z;-x',-y'), \quad (20)$$

$$\Phi_z(x,y,z;x',y')=-\Phi_z(x,y,z;-x',-y'). \quad (21)$$

Consequently, since the integration in the definition of E_x, E_y, and E_z are over a domain symmetric in x' and y', from equations (13)–(15) it follows that:

$$E_x(x,y,z)=-E_x(-x,-y,z), \quad (22)$$

$$E_y(x,y,z)=-E_y(-x,-y,z), \quad (23)$$

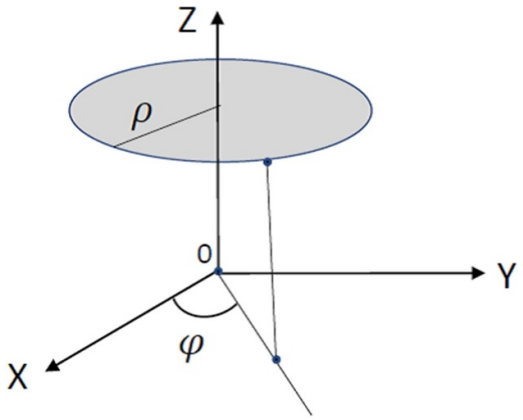

Figure A1. Reference frame used for the analysis of the cylindrical symmetry of the electric field $E(r)$ created by a square distribution of holes. The angle φ, measured with respect to the x-axis, characterizes the position of the considered point on the circle of radius ρ, centered on the z-axis. In the case of a pure cylindrical symmetry, E_z and the modulus of the electric field are φ-independent.

$$E_z(x,y,z)=E_z(-x,-y,z), \quad (24)$$

showing that the electric field $E(r)$ in opposite points, on the same plane orthogonal to the axis of the hole, have the same components along the z-axis, and opposite components along x and y axes.

To investigate the symmetry of the electric field, it is useful to analyze the dependence of the cartesian components of the electric field $E(r)$ on the azimuthal angle φ, and on the distance from the axis, ρ, shown in figure A1.

In figure A2 are reported the components of the electric field E_x, red, E_y, green, and E_z, black, versus φ, on a plane at a distance $z=R$ from the plane containing the hole, at a distance from the axis of the hole (a) $\rho=0.7\times R$ and (b) $\rho=1.5\times R$. On this circle, $x=\rho\cos\varphi$ and $y=\rho\sin\varphi$, and $z=R$.

From figure A2, the cylindrical symmetry of the electric field $E(r)$ is evident. In particular, E_z is constant on the circle of radius ρ centered on the axis of the hole, on a plane parallel to the plane of the hole. Also the modulus of the electric field is constant on the same circle.

The cylindrical symmetry discussed above is valid only in the case of a single hole in the PixE. When a distribution of holes, forming a square lattice of spatial periodicity a is considered, the cylindrical symmetry has to be re-analyzed. In fact, operating as before we have:

$$E_x(x,y,z)+E_x(-x,-y,z)=k\int_{-R}^{R}\mathrm{d}x'\int_{-\sqrt{R^2-x'^2}}^{\sqrt{R^2-x'^2}}\times\sum_{i,j}\Phi_x^{ij}(x,y,z;x',y')\,\mathrm{d}y', \quad (25)$$

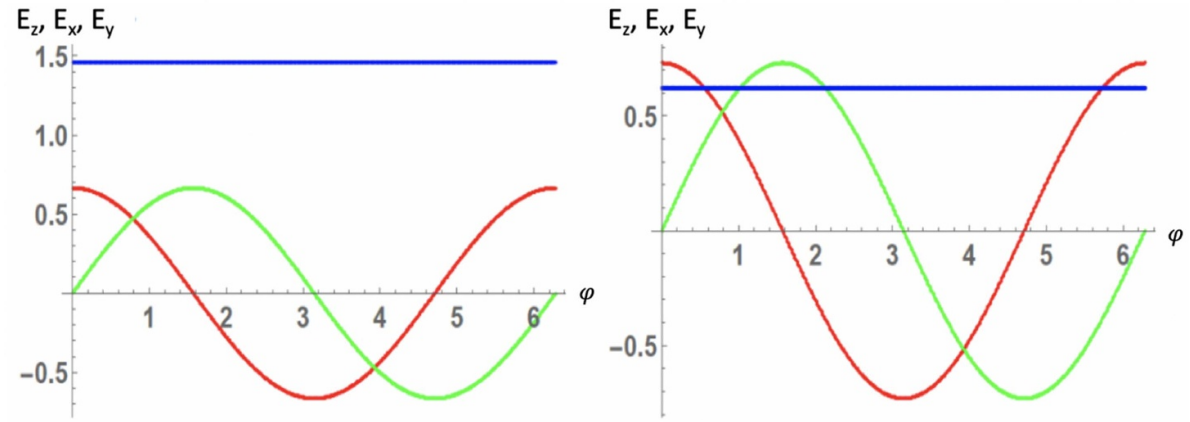

Figure A2. Cartesian components E_x, E_y and E_z of the electric field $E(r)$ created by a disc uniformly charged versus the azimuthal angle φ from the x-axis on a plane parallel to the (x,y)-plane.

$$E_y(x,y,z)+E_y(-x,-y,z)=k\int_{-R}^{R}\mathrm{d}x'\int_{-\sqrt{R^2-x'^2}}^{\sqrt{R^2-x'^2}}\times\sum_{i,j}\Phi_y^{ij}(x,y,z;x',y')\;\mathrm{d}y', \tag{26}$$

$$E_z(x,y,z)-E_z(-x,-y,z)=k\int_{-R}^{R}\mathrm{d}x'\int_{-\sqrt{R^2-x'^2}}^{\sqrt{R^2-x'^2}}\times\sum_{i,j}\Phi_z^{ij}(x,y,z;x',y')\;\mathrm{d}y', \tag{27}$$

where, as it follows from (9)–(11),

$$\Phi_x^{ij}(x,y,z;x',y')=\frac{x-x'-ia}{\left[(x-x'-ia)^2+(y-y'-ja)^2+z^2\right]^{3/2}}-\frac{x+x'+ia}{\left[(x+x'+ia)^2+(y+y'+ja)^2+z^2\right]^{3/2}},$$

$$\Phi_y^{ij}(x,y,z;x',y')=\frac{y-y-ja'}{\left[(x-x'-ia)^2+(y-y'-ja)^2+z^2\right]^{3/2}}-\frac{y+y'+ja}{\left[(x+x'+ia)^2+(y+y'+ja)^2+z^2\right]^{3/2}},$$

$$\Phi_z^{ij}(x,y,z;x',y')=\frac{z}{\left[(x-x'-ia)^2+(y-y'-ja)^2+z^2\right]^{3/2}}-\frac{z}{\left[(x+x'+ia)^2+(y+y'+ja)^2+z^2\right]^{3/2}}$$

at a distance $z=R$. E_x, red, E_y, green, E_z, blue. The distance from the axis of the hole is (a) $\rho=0.7\times R$ and (b) $\rho=1.5\times R$.

In the present case, a simple calculation shows that:

$$\Phi_x^{ij}(x,y,z;x',y')\neq-\Phi_x^{ij}(x,y,z;-x',-y'), \tag{28}$$

$$\Phi_y^{ij}(x,y,z;x',y')\neq-\Phi_y^{ij}(x,y,z;-x',-y'), \tag{29}$$

$$\Phi_z^{ij}(x,y,z;x',y')\neq-\Phi_z^{ij}(x,y,z;-x',-y'). \tag{30}$$

However, if the summation is performed on a symmetric interval for i and j:

$$\sum_{i,j=-N}^{N}\Phi_x^{ij}(x,y,z;x',y')=-\sum_{i,j=-N}^{N}\Phi_x^{ij}(x,y,z;-x',-y'), \tag{31}$$

$$\sum_{i,j=-N}^{N}\Phi_y^{ij}(x,y,z;x',y')=-\sum_{i,j=-N}^{N}\Phi_y^{ij}(x,y,z;-x',-y'), \tag{32}$$

$$\sum_{i,j=-N}^{N}\Phi_z^{ij}(x,y,z;x',y')=-\sum_{i,j=-N}^{N}\Phi_z^{ij}(x,y,z;-x',-y'). \tag{33}$$

Consequently, as in the previous case, relevant to a single hole, the electric field in opposite points, on the same plane orthogonal to the axis of the hole, have the same components along the z-axis, and opposite components along x and y axes. This conclusion holds if border effects can be neglected, as we assume in the following.

In figure A3, we show the cartesian components E_x, E_y and E_z of the electric field $E(r)$ due to a distribution of holes, on a plane parallel to the electrode with holes, at a distance $z=R$, on a circle of radius $\rho=0.7\times R$ (a) and $\rho=1.5\times R$ (b) centered on the axis of a hole, respectively. As in figure A1 the angle φ is measured with respect to the x-axis. These figures show that the symmetry is no longer cylindrical because E_z as well as E are not uniform on the circle of radius ρ, centered on the z-axis, and perpendicular to it. The interference between the different holes is responsible for a φ dependence of E_z

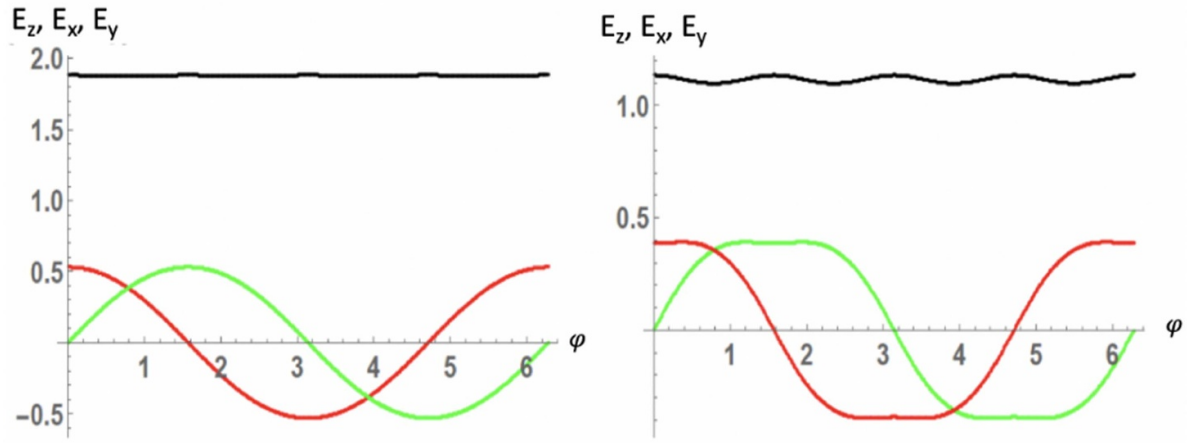

Figure A3. Cartesian components E_x, E_y and E_z of the electric field $E(r)$ created by a distribution of discs uniformly charged, forming a squared lattice of spatial periodicity (a) versus the azimuthal angle φ from the x-axis on a plane parallel to the (x,y) plane and a distance $z = R$. The distance from the axis of the hole is (a) $\rho = 0.7R$ and (b) $\rho = 1.5R$.

and E. However, the interference effect is rather small, and for practical application, it can be neglected. For the case shown in figure A3, it is smaller than 3% on E_z. This result is of some importance for what concerns the interaction of the electric field with the nematic LC as discussed above.

ORCID iDs

Giovanni Barbero https://orcid.org/0000-0002-2282-9536
Przemysław Morawiak https://orcid.org/0000-0003-3998-3422
Wiktor Piecek https://orcid.org/0000-0002-7683-535X

References

[1] Yang D K and Wu S T 2015 *Fundamentals of Liquid Crystal Devices* 2nd edn (Hoboken, NJ: Wiley)
[2] Lu R, Shua X, Wu S T, Hong Q and Wu T 2005 *J. Disp. Technol.* **1** 3
[3] Chen J, Cranton W and Finn M (eds) 2016 *Handbook of Visual Display Technology* (Berlin: Springer) (https://doi.org/10.1007/978-3-319-14346-0)
[4] Schadt M, Seiberle H and Schuster A 1996 Optical Patterning of multi-domain liquid crystal displays with wide viewing angles *Nature* **381** 212
[5] Lu R and Wu S-T 2006 *J. Disp. Technol.* **2** 217
[6] Gou F, Chen H, Li M-C, Lee S-L and Wu S-T 2017 *Opt. Express* **25** 7984
[7] Choi W-K, Hsu C-W, Tung C-H and Tseng B-K 2019 *Opt. Express* **27** 34343
[8] Komitov L US Patent 7 876 385
[9] Komitov L and Ibn-Elhaj M 2020 Fountain (FE-FFS) technology for wide viewing angle LCD *27th Proc. Int. Display Workshops Virtual Conf.* (*9–11 December 2020*) vol 27 pp 26–27
[10] Komitov L and Elhaj M I ref. WO2021105285A1
[11] Xiang C Y, Sun X W and Yin X J 2004 *J. Phys. D: Appl. Phys.* **37** 994
[12] Kim K-H, Yu B-H, Choi S-W, Oh S-W and Yoon T-H 2012 *Opt. Express* **20** 24376
[13] Landau L and Lifchitz E 1969 *Electrodymanique des milieu continus* (Paris: Mir)